Photovoltage transients at fullerene-metal interfaces

A. Podolian, V. Kozachenko, A. Nadtochiy, N. Borovoy, and O. Korotchenkov[a)]
Department of Physics, Taras Shevchenko Kyiv National University, Volodymyrska Street 64, Kyiv 01601, Ukraine

(Received 6 January 2010; accepted 25 March 2010; published online 6 May 2010)

Photovoltage (PV) transients are studied in C_{60}–Pb and C_{60}–Au thin films. The morphology of the C_{60} layers is characterized by x-ray diffraction and atomic force microscopy, which evidence the formation of a nanocrystalline C_{60} layer on polycrystalline Pb and Au underlayers. In contrast to Au substrate, Pb crystallites with a (111) texture are predominantly formed. The signs of the PV signals developed at the C_{60}–Pb and C_{60}–Au interfaces are found to be opposite due to very different workfunction values of the two metals. The evolution of the PV rise and decay curves with increasing light illumination intensity is completely different at the C_{60}–Pb and C_{60}–Au interfaces. The rise for the C_{60}–Pb interface speeds up considerably with the increase in intensity, which is markedly different from the behavior at C_{60}–Au, which exhibits nearly unchanged curve shapes. The PV decay time for C_{60}–Au is also only weakly affected by varying light intensity. In contrast, increasing the illumination intensity causes the decay curves for C_{60}–Pb to become multiexponential profiles, developing fast initial decays. The results are discussed in terms of different charge redistribution properties of C_{60} molecules adsorbed on Pb(111) and Au interfaces. The observed transformation of the PV decay curves is explained by the presence of interface states and a subsequent interplay of the charge redistribution properties of C_{60} molecules adsorbed on Pb(111). The results can be applied to sandwich structures containing organic-metal interfaces to account correctly for the interfacial charge transfer dynamics. © *2010 American Institute of Physics*. [doi:10.1063/1.3407562]

I. INTRODUCTION

Currently there is broad scientific and technological interest in exploring the possibility of using molecular materials in a wide range of optoelectronic devices, including organic light-emitting diodes and field-effect transistors, as well as photodetectors and solar cells.[1] Carbon-based nanomaterials such as fullerenes have been the focus of a great deal of effort in the past decade due to their promising use in future nanodevices. In particular, fullerenes have attracted attention as materials that combine the electronic and optical properties of semiconductors with cheap processing advantages such as coating and processing on large areas.

The interfaces of C_{60} films with metal surfaces are of particular interest for molecular electronics applications.[2] The performance of sandwich devices, including organic layered structures, is known to be critically dependent on the nature of the metal top electrode.[3] Recently, electron-rich and C_{60} compounds such as C_{60}-metal sandwich complexes have been exploited to achieve strong electronic communication in the molecular chains.[4,5] Coupled with self-assembled multilayered thin films with potential gradients, these systems have shown promise in mimicking natural photosynthetic apparatus and fabricating efficient photovoltaic cells.[5,6] In many cases, the charge transfer across C_{60}-metal interfaces plays an important role for applications, generating a large volume of research devoted to the properties of these interfaces.[7–10]

Undoped C_{60} films have low mobilities, typically about 10^{-3} $cm^2/V\,s$ at room temperature,[11] and the charge transport is dominated by thermally activated hopping processes. Since the low carrier mobility implies a mean free path of the order of the interatomic distances, the sandwich system including C_{60} thin films may be used as a model system for studying the electric transport behavior in the nanoparticle interconnect networks.

Transient photovoltage (PV) has proven to be a useful tool for gaining more insight into the basic physical processes that accompany photogeneration of charge carriers in sandwich organic devices. Thus, the transient PV signals in thin films of poly(*p*-phenylenevinylene) (PPV), 1,7-bis-(*N*,*N*-dimethylamino)heptamethineperchlorate, and phthalocyanine (Pc) can be of different polarities, resulting from different diffusion coefficients and lengths of electrons and holes.[12–14] The magnitude, polarity, and response time of transient PV taken in the Al/tin-Pc/indium-tin-oxide (ITO) sandwich cell are found to depend on the intensity and wavelength of the incident light, which offers a potential application in the area of light-controlled nonlinear optoelectronic detectors.[15] Transient PV measured from the device of ITO/*N*,*N*′-Bis(naphthalene-1-yl)-*N*,*N*′-bis(phenyl) benzidine (NPB)/Al and of ITO/C_{60} exhibits an abnormal polarity change from negative to positive upon pulsed laser irradiation, related to the carrier separation at the ITO-NPB and at the ITO-C_{60} interface.[16,17] The process of exciton dissociation at the interface between ITO and poly(2-methoxy-5-(2′-ethylhexyloxy)-1, 4-phenylenevinylene) has been studied using transient PV.[18] The transient PV signals of the ITO/polymer (microporous metal-organic framework)/ITO sandwich cell exhibit retardation in time, which results

[a)]Electronic mail: olegk@univ.kiev.ua.

from a slow diffusion of excess electrons and holes indicative of the diffusion PV transient.[19] In trap limited devices, such as dye-sensitized solar cells, transient PV measurements offer the relationship between the charge transport rate and charge density, consistent with the trap limited charge transport model.[20] Transient PV measurements are employed to determine the mechanism for the improved photovoltaic characteristics of a solar cell consisting of dye molecules chemisorbed on a porous, nanocrystalline TiO_2 film.[21,22] Transient PV is also applicable to a hydroxyl-terminated silicon surface, used as a substrate for fabricating molecular electronics interfaces.[23]

In this work, we study the temporal behavior of the photoinduced charge at fullerene-metal interfaces by employing PV transients. Two metals having very different workfunctions (Pb and Au) are used, allowing either the accumulation or depletion of the near-interface region of the C_{60}-metal system with photoexcited electrons and holes, thus effectively modifying the transient characteristics of the PV signal.

II. EXPERIMENTAL DETAILS

The C_{60}-metal sample was structured as follows. A 1 μm thick Pb or Au layer was formed on the mirror-polished Al substrate for the subsequent deposition of a C_{60} film. The metals and fullerenes were vacuum-evaporated from simple sources, consisting of tungsten crucibles with shutters heated by an electric current. The crucibles were filled with a 99.99% purity metal (Pb or Au) and a 99.9% purity C_{60} powder. The first step consisted of the metal film deposition, which served as a freshly prepared substrate for the sequential deposition of C_{60}. The pressure in the vacuum chamber was about 10^{-5} Torr. The temperature in the crucible with a C_{60} powder was 450 °C, whereas the substrate was kept at 20 °C. The deposition rate of C_{60} was about 10 nm/s. The thickness of the deposited layer was determined using a calibrated optical sensor.

X-ray diffraction (XRD) analysis was performed in a step-scanning mode [$\Delta(2\theta)=0.03°$, accumulation time =15 s], using Fe $K\alpha_{1,2}$ radiation and a $\theta-2\theta$ diffractometric instrument, equipped with a Ge(111) monochromator in the incident beam and scintillation counter detection. Instrumental full width at half-maximum (FWHM) broadening was about 0.1° (measured at $2\theta=32.70°$ using a silicon single-crystal reference).

Fourier transformed-infrared (FTIR) spectra were obtained using a Nicolet model 6700 FTIR spectrometer. The transmission spectra were taken from the C_{60} layer deposited onto the transparent mica foil, and the conditions used during growth were the same as those employed for preparing the C_{60}-metal samples.

Figure 1 presents the experimental setup used to measure the PV. PV transients were measured in the capacitor arrangement.[24–26] The incident light, produced by a light-emitting diode (LED light in Fig. 1) with a peak wavelength of 406 nm, was chopped and passed through a transparent quartz plate (1 in Fig. 1). A parallel plate capacitance was formed between a metal net electrode (2) and the sample (3),

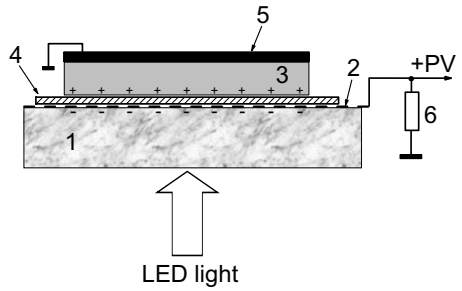

FIG. 1. Schematic diagram of the experimental setup for transient PV measurements. 1—transparent quartz plate, 2—metal net electrode, 3—C_{60}-metal sample, 4—20 μm mica insulating foil, 5—Al electrode, and 6—output resistance. The appearance of a positive PV signal (+PV) due to a positive charge developed in the C_{60} layer and the appropriate negative charge occurring in the net electrode is exemplified.

separated by a mica insulating foil (4) with a thickness of about 20 μm. A grounded Al electrode (5) was slightly pressed against the bottom layers with a stainless spring. A 1 G Ω load resistor (6), a high-impedance buffer cascade (input resistance 10^{12} Ω, output resistance 50 Ω) based on a field-effect transistor, and a 20 MHz sampling oscilloscope were used in the measurements. The measuring circuit was carefully screened to ensure the experimental system was not susceptible to electronic pickups or ground loop effects.

The output signal can be related to the input PV produced in the C_{60}-metal structure by utilizing an equivalent circuit of the structure with the buffer cascade, which is shown in the inset of Fig. 2. Here, U_{PV} is the PV generated in the C_{60}-metal structure, R_S is the structure resistance, C_m is the net electrode-sample capacitance, R_i is the parallel resistance of the buffer cascade input and the PV cell output loads, and C_i is the input capacitance of the buffer cascade, including the coaxial cable capacitance. Then the output signal ΔU is

$$\Delta U = \frac{\omega C_m R_i U_{PV}}{\omega C_m R_S + \omega C_i R_i + \omega C_m R_i + j(\omega^2 C_i C_m R_i R_S - 1)}, \tag{1}$$

where j is the imaginary unit, $\omega=2\pi f$, and f is the light chopping frequency. It is seen that the measured PV (ΔU) differs from that produced in the C_{60}-metal structure (U_{PV}), and the difference is the chopping frequency dependent (see

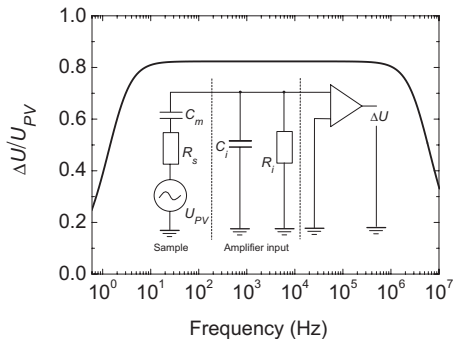

FIG. 2. Frequency-dependent ratio of the experimentally measured (ΔU) and generated in the C_{60}-metal structure (U_{PV}) PV. Inset: equivalent circuit of the C_{60}-metal structure for measuring the PV. In our experimental setup, $R_S=100$ Ω, $C_m=70$ pF, $R_i=1$ G Ω, and $C_i=15$ pF.

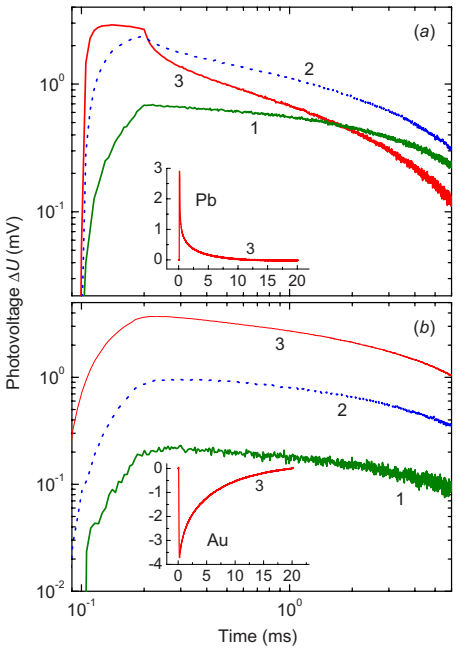

FIG. 3. (Color online) Time-dependent PV of C_{60} thin film grown on (a) Pb and (b) Au at illumination intensity of about 2 (1), 20 (2), and 200(3) mW cm^{-2}. The LED peak wavelength is 406 nm. Note that the PV signal is positive in panel (a) and negative in panel (b) (insets). It is reversed when plotted on a log scale in panel (b).

Fig. 2). The frequency f used in the experiments was then chosen to fall into the horizontal part of the curve of Fig. 2, providing $\Delta U = 0.823 U_{PV}$. It may also be seen from Fig. 2 that the PV decay times ranging from 0.3 μs to 70 ms can be detected by the circuitry without changing the shape of the PV decay curve. Pulse lengths of 100 μs were used in the measurements, with rise and fall times of $\leq$0.5 μs.

The decay transients stored in the computer memory can then be averaged as many times as required to achieve a given signal-to-noise ratio, and averaging of ten consecutive transients was typically used. The light intensity was calibrated by an optical power meter. The LED was controlled by the external bias in the form of square-function pulse. Because of the low illumination intensity employed in this work, irreversible photochemical effects were not likely to occur in the C_{60} layers. All measurements were made in air at room temperature. A slow degradation of the PV signal size was observed in our C_{60}-metal samples, which, however, was observed to be slow enough to allow reproducible measurements.

III. RESULTS AND DISCUSSION

Figure 3 contrasts the typical PV transients for C_{60}–Pb and C_{60}–Au films taken at different illumination intensities. The commensurate signs of the PV signals developed at the C_{60}–Pb and C_{60}–Au interfaces are opposite, as seen in the insets. In agreement with the electrical circuitry shown in Fig. 1, the observed PV signs indicate that positive (negative) charges are accumulated in the C_{60} film for the C_{60}–Pb (C_{60}–Au) interfaces.

Of importance is the fact that the evolution of the PV rise with increasing LED illumination intensity I_{LED} is completely different at the C_{60}–Pb and C_{60}–Au interfaces, as exemplified by curves 1 to 3 in Figs. 3(a) and 3(b), respectively. First, the rise is remarkably faster for the C_{60}–Pb interface. Second, it speeds up considerably with increasing I_{LED} in C_{60}–Pb [1 to 3 in Fig. 3(a)]. However, this is not observed in C_{60}–Au. As can be seen in Fig. 3(b), the rise time remains almost unaffected in curves 1 to 3. Third, at high enough I_{LED}, the PV rise in C_{60}–Pb rapidly achieves a peak value with a subsequent signal decrease [3 in Fig. 3(a)], which is not reproduced in C_{60}–Au [Fig. 3(b)].

The PV decays taken after the LED light was off (see after 0.2 ms in Fig. 3) are also different for the C_{60}–Pb and C_{60}–Au interfaces. At low I_{LED}, the decays look close to linear on a semilog scale, signifying exponential decays. Again, the decay time is weakly affected with increasing I_{LED} for C_{60}–Au, so that a nearly parallel shift in the linear plot of log PV versus time takes place [the decay times of 11.5 ms, 8.4 ms, and 7.0 ms for curves 1, 2, and 3, respectively, are obtained from Fig. 3(b)]. The PV transient for C_{60}–Pb also decays exponentially with the time constant of 6.2 ms at low I_{LED} [curve 1 in Fig. 3(a)]. Meanwhile, increasing the illumination intensity develops considerably faster initial decays, which are seen in curves 2 and 3 of Fig. 3(a) in addition to slower decays of of 4.9 ms and 3.6 ms for curves 2 and 3, respectively, of Fig. 3(a). At times shorter than $\approx$2 ms, these fast decays can be nicely approximated by two exponents with 80 and 720 μs (curve 2) and 35 and 420 μs (curve 3).

To track the origin of the PV transients, the major photovoltaic mechanisms in organic sandwich materials,[19,27–31] nanocrystalline films, including materials with a very large Maxwell relaxation time due to a high electrical resistivity,[17,32–34] and the effects of adsorption of C_{60} molecules on the Pb and Au surfaces[7–10] have to be taken into account. The photovoltaic performance of the structure can also be significantly affected by the layer morphology.[35–37]

The morphology and crystallinity of the prepared C_{60}-metal sandwich structures have been studied using XRD, atomic force microscopy (AFM), and FTIR spectroscopy. Figure 4 shows the XRD patterns of C_{60}–Pb and C_{60}–Au thin films. The intensities of the diffracted x-rays are normalized by the layer thicknesses. It is assumed that the C_{60} and metal layer thicknesses are thin well enough compared with the value of absorption length of the Fe $K\alpha_{1,2}$ line for C_{60}, Pb, and Au. Therefore, the diffraction profiles in panels (a) and (b) of Fig. 4 are comparable.

The broad diffraction peaks at 2θ values of about 26° are observed in panels (a) and (b) of Fig. 4, matching the (220) and (311) crystalline planes of C_{60}.[38,39] The broad nature of the XRD peaks can be attributed to the nanocrystalline nature of C_{60} grains. The coherent length corresponding to the dimensions of the crystalline grains is calculated from the FWHM of the XRD peak β (in rad), using the Debye–Scherrer equation[40]

$$\tilde{L} = \frac{0.9\lambda}{\beta \cos \theta}, \tag{2}$$

where λ is the x-ray wavelength. The shape of the (220) and (311) XRD peaks is approximated by a Voigt function, a

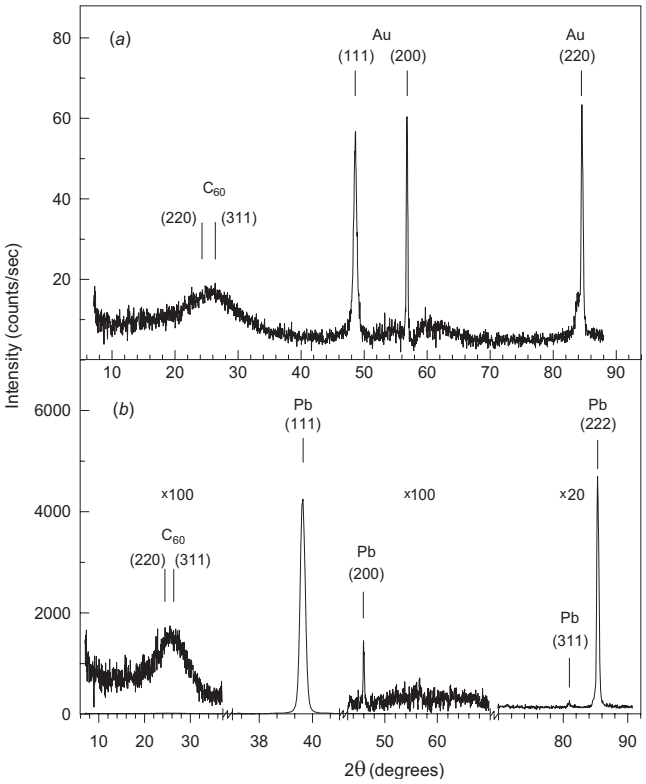

FIG. 4. XRD profiles for (a) C_{60}–Au and (b) C_{60}–Pb thin films, exhibiting the patterns of C_{60} and the metal layers. The XRD profile of the Al substrate has been subtracted from the data.

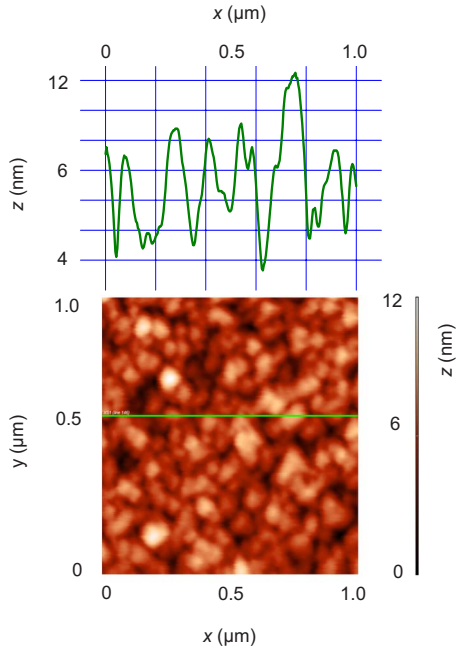

FIG. 5. (Color online) AFM image taken from a C_{60}–Au film and the cross-sectional view taken along the line shown in the image. The cross-section gives a root-mean-square roughness of 1.8 nm. The image is obtained using an NT-MDT NTEGRA Prima Scanning Probe Microscope run in the semicontact AFM mode.

convolution of a Lorentzian and a Gaussian that describe homogeneous and inhomogeneous broadening, respectively. Although this is obviously a simplified line shape, which neglects the contribution of high-order effects, we find that it gives a very good fit to the measured C_{60} peaks when taking β to be the same for the (220) and (311) peaks and equal to $(1.7 \pm 0.2)°$. The resulting value is $\tilde{L}=(7 \pm 2)$ nm.

After the XRD measurement, AFM images were obtained. As observed in Fig. 5, the surface of the C_{60} layer is rough, consisting of small grains with an average diameter of $\approx$60 nm. A root-mean-square roughness of the surface, determined by AFM, is found to be up to $\approx$2 nm, which is nearly consistent with the coherent length $\tilde{L}$ determined from XRD. Therefore, the grains can be supposed to be clusters that should be an assembly of the nanocrystalline particles formed by compacted fullerene molecules.

Since after the sample deposition the C_{60} was transferred into the XRD and PV measuring setup exposed to air, oxygen contamination of the material might be expected to occur. Likewise, the C_{60} layers grown on a mica substrate would also be affected by oxygen in a similar way. However, characteristic infrared absorption peaks of an isolated C_{60} molecule[41–43] are very clearly discernible at 1183, 1429, and 1462 cm^{-1} in the absorption spectrum shown in Fig. 6, also taken after sample exposure to air. This allowed us to assume that the fullerene shell was not destroyed during the layer deposition and that the oxygen molecules were only weakly interacting with the C_{60} molecules.

Figure 4 also shows the XRD patterns of Pb and Au films, indicating that the metal layers are polycrystalline. As can be seen in panel (b), the intensity of the Pb(111) peak is more than two orders of magnitude greater than those of the Pb(200) and Pb(311) peaks, whereas the intensities of the Au(111), Au(200), and Au(220) peaks are comparable [panel (a)]. Therefore, in contrast to Au films, Pb layers have a strong (111) texture, exhibiting a predominantly aligned growth of the Pb crystallites with (111) planes parallel to the Pb film surface.

Thus, the key assumption from the XRD, AFM, and FTIR measurements is that the nanocrystalline phase is preserved over the entire C_{60} layer and the roughness of the C_{60} surface in Fig. 5 is probably due to compacted clusters, but without disintegration of the fullerene molecules.

A consequence of the multigrain structure observed in Fig. 5 can be the occurrence of charge density regions and Schottky barriers induced by grain boundaries.[44] This may produce PV signals due to the separation of photogenerated

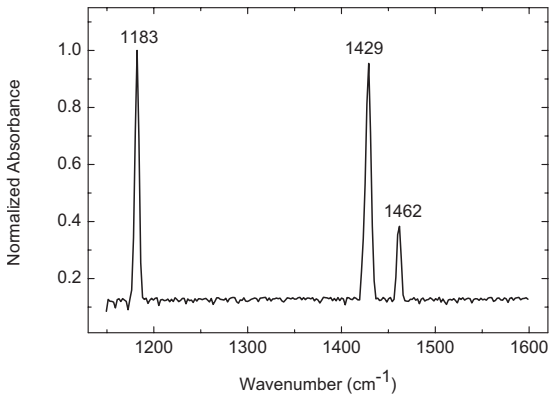

FIG. 6. FTIR spectrum of a C_{60} film grown on a 20 μm thick mica substrate.

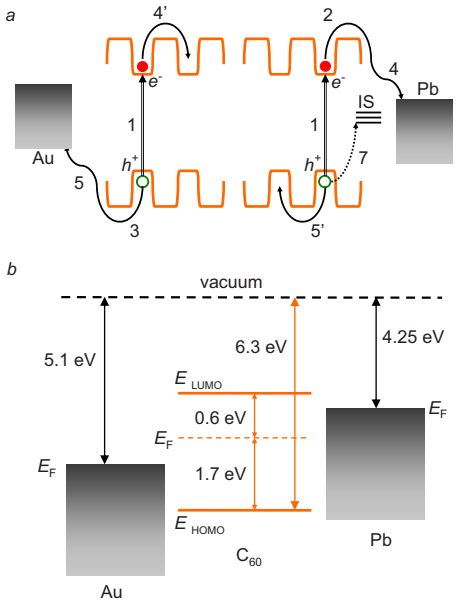

FIG. 7. (Color online) (a) Sketch of the major processes involved into the PV generation. HOMO and LUMO indicate the highest occupied and the lowest unoccupied molecular orbitals, respectively. Dips schematically illustrate the barriers for charge transport between individual C_{60} cages. (b) The energy level alignment in the spatially separated C_{60}–Pb and C_{60}–Au materials. The work functions are W_f=4.25 eV, (Ref. 45) 4.6 eV (Ref. 46), and 5.1 eV (Ref. 46) in Pb, C_{60}, and Au, respectively.

carriers at the barriers. Additionally, different kinds of trap sites are likely to occur at the grain boundaries, which may slow down the observed PV decay transients, in agreement with sufficiently large characteristic decay times observed in Fig. 3. However, it has been verified that the PV sign, size and transient shapes remain nearly unaffected by varying the thickness of the C_{60} layers from 50 to 300 nm. This brings up an important point, that the PV signal observed in our samples is predominantly formed at the C_{60}-metal interface.

The PV would then be sensitive to the orientational state of the C_{60} molecules with respect to the supporting metal layer, and to the electronic structure of the C_{60}–Pb(111) and C_{60}–Au with respect to the likely charge transfer effects occurring at the interfaces.

At the photon energy of the LED light used in this study (3 eV) a direct photogeneration of free electrons and holes [process 1 in Fig. 7(a)] takes place.[47] The interconnection between individual C_{60} nanocrystals allowing charge transfer through the potential barriers separating them is likely to achieve a separation of the electrons and holes in the built-in electric fields developed at the interfaces. Then the LED light would induce a nonnegligible change in the fields, producing a PV signal.

If other processes are assumed unimportant, one can assume that Pb gives electrons to C_{60} whereas Au turns out to accept electrons from C_{60}. The supporting evidence is shown in Fig. 7(b), illustrating the energy level diagrams of C_{60}–Pb and C_{60}–Au when the vacuum levels in all the materials are adjusted before they are brought together. The Fermi energy level in Au being lower than that in C_{60} forces electrons to move to the Au electrode after the C_{60}–Au contact is formed, leading to the built-in electric field directed from C_{60} to Au. Hence, the photoexcited holes would move to the Au electrode and the C_{60} becomes negatively charged, providing the negative PV, as indeed observed in the inset of Fig. 3(b). In contrast, the Fermi energy level in Pb is higher than that in C_{60} [Fig. 7(b)], which finally leads to the built-in electric field directed from Pb to C_{60} and positive PV observed in the inset of Fig. 3(a). Therefore, according to this simple model, photoexcited electrons [process 2 in Fig. 7(a)] and holes (process 3) move to the Pb or Au electrodes, respectively. A consequence is that the mobile electrons and holes escape from the interface region in the processes 4, 4′ and 5, 5′, respectively, forming the PV signals discussed above.

In the general case of the spatially distributed positive and negative charge carriers, the time (t)-dependent PV signal is[34]

$$U_{\mathrm{PV}}(t) = \frac{e}{\varepsilon\varepsilon_0} N(t)[\langle r_n\rangle(t) - \langle r_p\rangle(t)], \tag{3}$$

where e is the elementary charge, ε_0 is the permittivity of free space, ε is the dielectric constant of the C_{60} layer, $N(t)$ is the total number of the photoinjected electrons (or holes) per unit area, and $\langle r_n\rangle(t)$ and $\langle r_p\rangle(t)$ are the centers of negative and positive charge, respectively. Considering the charge separation length to be $\langle r_n\rangle(t)-\langle r_p\rangle(t)$, the rise and decay of the PV are controlled by the spatial separation length of the oppositely charged carriers and the number of carriers $N(t)$.

At low I_{LED}, the transients of the PV are determined by the charge separation lengths occurring over distances given by the processes 4–5′ and 4′–5 in Fig. 7(a). Consequently, a fairly similar PV(t) behavior is exhibited in curves 1 of Figs. 3(a) and 3(b). The reason for shortening the rises and decays in curves 2 and 3 of Fig. 3(a) is that the competition between separation of electrons and holes [processes 4–5′ and 4′–5 in Fig. 7(a)] and the Coulomb attraction of electrons and holes may give rise to decreasing $\langle r_n\rangle(t)-\langle r_p\rangle(t)$ under enhanced $N(t)$ with increasing I_{LED}. Once high enough electron density is injected in process 4 in Fig. 7(a) [rapid rise in curve 3 of Fig. 3(a)], a part of the photoexcited holes attracted by the resulting negative charge is captured at the interface states IS [process 7 in Fig. 7(a)]. This results in the PV decrease between ≈0.13 and 0.2 ms and a subsequent faster decay in curve 3 of Fig. 3(a) due to the decreasing separation lengths in Eq. (3) and subsequently increasing overlap of the wave functions of electrons in Au and holes at IS.

It may be suggested that, for the C_{60}–Au interface, the photoexcited electrons with a considerably higher mobility than that of holes rapidly escape away from the interface [process 4′ in Fig. 7(a)], preventing their backward motion to the Au layer. Consequently, there is no $\langle r_n\rangle(t)-\langle r_p\rangle(t)$ decrease with increasing I_{LED}, resulting in the observation that the transient shapes are nearly similar in curves 1 to 3 of Fig. 3(b).

Consistent with the expectation that decreasing the distance between the centers of charge of the positive and negative carriers quenches the PV, the data of Fig. 3 exhibit such a behavior. Thus, the peak PV values for the C_{60}–Pb interface are ≈0.7 mV and 2.9 mV in curves 1 and 3 of Fig. 3(a),

respectively, showing a four times increase in PV, whereas those for the C_{60}–Au interface amount to ≈0.2 mV and 3.7 mV in curves 1 and 3 of Fig. 3(b), respectively, exhibiting a PV increase by 18.5 times. It is seen that, at low I_{LED}, the PV signal for the C_{60}–Pb interface is greater than that for C_{60}–Au (0.7 mV and 0.2 mV, respectively), illustrating the greater charge separation length that occurs in C_{60}–Pb. This gradually becomes smaller than that in C_{60}–Au with increasing I_{LED}, as expected in the above picture.

The appearance of these differences is obviously due to the nature of the C_{60}-metal regions that contribute to the PV. It is known that one of the most fundamental properties of C_{60} electronic structure is the energy location of the lowest unoccupied molecular orbital (LUMO) and highest occupied molecular orbital (HOMO) states, E_{LUMO} and E_{HOMO}, respectively, both of which can be changed by substrate-induced charging effects. Charge transfer, intramolecular Coulomb energy (U), and screening effects all play an important role in determining the HOMO and LUMO level structure of adsorbed C_{60}. Thus, intramolecular Coulomb repulsion changes the energy required for electrons to be either added or removed from an adsorbed molecule, increasing observed HOMO-LUMO gaps (ΔE_{HL}) by U (Ref. 9)

$$\Delta E_{HL} = E_{LUMO} - E_{HOMO} + U. \quad (4)$$

Screening by a substrate, however, tends to reduce Coulomb repulsion and thus also influences ΔE_{HL}.

It is therefore believed that the flow of charges reproduced by arrow 4 in Fig. 7(a) enhances the Pb substrate-induced screening effect, thus tending to reduce the C_{60} intramolecular Coulomb repulsion [reduced U in Eq. (4) due to increased screening] and to decrease the energy required to remove electrons from an adsorbed C_{60} molecule. This is in agreement with the speeding up of the PV rise observed in Fig. 3(a) and discussed above. In clear contrast, the reversed flow of charges through the C_{60}–Au interface [arrow 5 in Fig. 7(a)] tends to quench the screening effect, so that no I_{LED}-dependent speeding up is observed in Fig. 3(b).

This provides a rough explanation as to why the evolution of the PV transients with increasing I_{LED} is so different at the C_{60}–Pb and C_{60}–Au interfaces. This behavior is seemingly bolstered by the fact that the deposition of fullerenes on Pb and Au surfaces is fairly different with respect to the substrate-adsorbate interactions.[7–10] The deposition of submonolayer amounts of C_{60} onto a gold film showed that the interaction of the two species is mainly due to chemisorption of the first C_{60} monolayer. A constant band bending in the fullerene film is additionally detected with no charge transfer occurring from the Au to the C_{60} lowest unoccupied molecular orbital, as observed by the photoelectron spectroscopy in the ultraviolet.[8] The adsorption of C_{60} on Au(111) and Au(110) suggests a commensurate molecular layer oriented along directions parallel to the Au atomic rows.[10,48] Although the nature of the bonding between the C_{60} molecules and the Pb(111) is not yet known, scanning tunneling microscopy experiments indicate a relatively weak C_{60}–Pb interaction compared with other metals.[7,10,49,50] This weakly interacting adsorption system reveals two coexisting close-packed structures for a C_{60} monolayer on Pb(111), yielding two different alignments of the LUMO with respect to the Pb Fermi level.[7] In this case, the higher LUMO alignment can be associated with molecules on top sites, which may be higher than, for example, molecules on hollow sites, according to the model of screening of local charges in molecules by metal surfaces,[51] because the LUMO peak is expected to appear at higher energy positions in molecules lying higher from the Pb surface. Therefore, it would be logical to speculate that the C_{60} molecules lying closer to the Pb surface act as the interface states IS capturing photoexcited holes in the process 7 shown in Fig. 7(a).

IV. CONCLUSIONS

In summary, we present PV transients taken at C_{60}–Pb and C_{60}–Au interfaces. We observe an evolution of the PV rise and decay curves with varying light illumination intensity, which is completely different for the two interfaces. We explain the results by the fact that the electronic properties of C_{60} molecules adsorbed on the Pb and Au surfaces are fairly different. The obtained results may be of interest for elucidating the charge separation processes at organic-metal interfaces and interfacial charge transfer dynamics, which are crucial for efficient conversion of solar energy into electrical energy in photovoltaic cells and for improving the functionality of sandwich organic LEDs, utilizing the coupling of the organic material to metal electrodes.

[1] N. Sariciftci and A. Heeger, *Handbook of Organic Conductive Molecules and Polymers* (Wiley, New York, 1997).
[2] M. C. Petty, *Molecular Electronics: From Principles to Practice* (Wiley, New York, 2007).
[3] V. D. Mihailetchi, L. J. A. Koster, and P. W. M. Blom, Appl. Phys. Lett. **85**, 970 (2004).
[4] K. Lee, H. Song, B. Kim, J. T. Park, S. Park, and M.-G. Choi, J. Am. Chem. Soc. **124**, 2872 (2002).
[5] Y.-J. Cho, T. K. Ahn, H. Song, K. S. Kim, C. Y. Lee, W. S. Seo, K. Lee, S. K. Kim, D. Kim, and J. T. Park, J. Am. Chem. Soc. **127**, 2380 (2005).
[6] D. M. Guldi, I. Zilbermann, G. Anderson, A. Li, D. Balbinot, N. Jux, M. Hatzimarinaki, A. Hirsch, and M. Prato, Chem. Commun. (Cambridge) **2004**, 726.
[7] H. I. Li, K. J. Franke, J. I. Pascual, L. W. Bruch, and R. D. Diehl, Phys. Rev. B **80**, 085415 (2009).
[8] H. Kröger, P. Reinke, M. Büttner, and P. Oelhafen, J. Chem. Phys. **123**, 114706 (2005).
[9] X. Lu, M. Grobis, K. H. Khoo, S. G. Louie, and M. F. Crommie, Phys. Rev. B **70**, 115418 (2004).
[10] A. J. Maxwell, P. A. Brühwiler, D. Arvanitis, J. Hasselström, M. K.-J. Johansson, and N. Mårtensson, Phys. Rev. B **57**, 7312 (1998).
[11] V. D. Mihailetchi, J. K. J. van Duren, P. W. M. Blom, J. C. Hummelen, R. A. J. Janssen, J. M. Kroon, M. T. Risoens, W. J. H. Verhees, and M. M. Wienk, Adv. Funct. Mater. **13**, 43 (2003).
[12] V. Duzhko, Th. Dittrich, B. Kamenev, V. Yu. Timoshenko, and W. Brutting, J. Appl. Phys. **89**, 4410 (2001).
[13] C. Damm, L. Dähne, and F. W. Müller, Phys. Chem. Chem. Phys. **3**, 5416 (2001).
[14] H. Tian and K. C. Chen, Dyes Pigm. **27**, 191 (1995).
[15] Y.-L. Pan, L.-B. Chen, Y. Wang, Y.-Y. Zhao, F.-M. Li, A. Wagiki, M. Yamashita, and T. Tako, Appl. Phys. Lett. **68**, 1314 (1996).
[16] Q. L. Song, H. R. Wu, X. M. Ding, X. Y. Hou, F. Y. Li, and Z. G. Zhou, Appl. Phys. Lett. **88**, 232101 (2006).
[17] X. Y. Sun, B. F. Ding, Q. L. Song, X. Y. Zheng, X. M. Ding, and X. Y. Hou, Appl. Phys. Lett. **93**, 063301 (2008).
[18] Q. Shi, Y. Hou, Y. Li, Z. Feng, and X. Liu, Phys. Lett. A **372**, 5853 (2008).
[19] Q.-R. Fang, G.-S. Zhu, M. Xue, Q.-L. Zhang, J.-Y. Sun, X.-D. Guo, S.-L. Qiu, S.-T. Xu, P. Wang, D.-J. Wang, and Y. Wei, Chem.-Eur. J. **12**, 3754 (2006).
[20] B. C. O'Regan, K. Bakker, J. Kroeze, H. Smit, P. Sommeling, and J. R.

Durrant, J. Phys. Chem. B **110**, 17155 (2006).
[21]N. Kopidakis, K. D. Benkstein, J. van de Lagemaat, and A. J. Frank, J. Phys. Chem. B **107**, 11307 (2003).
[22]A. J. Frank, N. Kopidakis, and J. van de Lagemaat, Coord. Chem. Rev. **248**, 1165 (2004).
[23]R. A. Murdick, R. K. Raman, Y. Murooka, and C.-Y. Ruan, Phys. Rev. B **77**, 245329 (2008).
[24]E. O. Johnson, J. Appl. Phys. **28**, 1349 (1957).
[25]R. S. Nakhmanson, Solid-State Electron. **18**, 617 (1975).
[26]C. Munakata, S. Nishimatsu, N. Honma, and K. Yagi, Jpn. J. Appl. Phys., Part 1 **23**, 1451 (1984).
[27]S. Nakade, Y. Saito, W. Kubo, T. Kanzaki, T. Kitamura, Y. Wada, and S. Yanagida, J. Phys. Chem. B **107**, 8607 (2003).
[28]S. Nakade, Y. Saito, W. Kubo, T. Kanzaki, T. Kitamura, Y. Wada, and S. Yanagida, J. Phys. Chem. B **108**, 1628 (2004).
[29]A. Green, E. Palomares, S. A. Haque, and J. R. Durrant, Proc. SPIE **5513**, 56 (2004).
[30]B. C. O'Regan and F. Lenzmann, J. Phys. Chem. B **108**, 4342 (2004).
[31]C. Goh, S. R. Scully, and M. D. McGehee, J. Appl. Phys. **101**, 114503 (2007).
[32]L. Kronik, N. Ashkenasy, M. Leibovitch, E. Fefer, Y. Shapira, S. Gorer, and G. Hodes, J. Electrochem. Soc. **145**, 1748 (1998).
[33]V. Duzhko, V. Yu. Timoshenko, F. Koch, and Th. Dittrich, Phys. Rev. B **64**, 075204 (2001).
[34]I. Mora-Seró, Th. Dittrich, G. Garcia-Belmonte, and J. Bisquert, J. Appl. Phys. **100**, 103705 (2006).
[35]*Organic Photovoltaics*, edited by S.-S. Sun and N. S. Sariciftci (Taylor & Francis, London, 2005).
[36]A. Moliton and R. C. Hiorns, Polym. Int. **53**, 1397 (2004).
[37]S. E. Shaheen, C. J. Brabec, N. S. Sariciftci, F. Padinger, T. Fromherz, and J. C. Hummelen, Appl. Phys. Lett. **78**, 841 (2001).
[38]F. Hebard, R. C. Haddon, R. M. Fleming, and A. R. Kortan, Appl. Phys. Lett. **59**, 2109 (1991).
[39]E. A. Katz, D. Faiman, S. Shtutina, N. Froumin, M. Polak, A. P. Isakina, K. A. Yagotintsev, M. A. Strzhemechny, Y. M. Strzhemechny, V. V. Zaitsev, and S. A. Schwarz, Physica B **304**, 348 (2001).
[40]B. D. Cullity and S. R. Stock, *Elements of X-Ray Diffraction*, 3rd ed. (Prentice-Hall, Englewood Cliffs, NJ, 2002).
[41]W. Krätschmer, L. D. Lamb, K. Fostiropoulos, and D. R. Huffman, Nature **347**, 354 (1990).
[42]G. Dresselhaus, M. S. Dresselhaus, and P. C. Eklund, Phys. Rev. B **45**, 6923 (1992).
[43]P. C. Eklund, A. M. Rao, P. Zhou, Y. Wang, and J. M. Holden, Thin Solid Films **257**, 185 (1995).
[44]T. B. Singh, N. S. Sariciftci, H. Yang, L. Yang, B. Plochberger, and H. Sitter, Appl. Phys. Lett. **90**, 213512 (2007).
[45]*CRC Handbook of Chemistry and Physics*, 90th ed., edited by D. R. Lide (CRC, Boca Raton, Florida, 2009).
[46]S. J. Kang, Y. Yi, C. Y. Kim, S. W. Cho, M. Noh, K. Jeong, and C. N. Whang, Synth. Met. **156**, 32 (2006).
[47]C. H. Lee, G. Yu, D. Moses, V. I. Srdanov, X. Wei, and Z. V. Vardeny, Phys. Rev. B **48**, 8506 (1993).
[48]C. Rogero, J. I. Pascual, J. Gómez-Herrero, and A. M. Baró, J. Chem. Phys. **116**, 832 (2002).
[49]R. Felici, M. Pedio, F. Borgatti, S. Iannotta, M. Capozi, G. Ciullo, and A. Stierle, Nat. Mater. **4**, 688 (2005).
[50]W. W. Pai, C. L. Hsu, M. C. Lin, K. C. Lin, and T. B. Tang, Phys. Rev. B **69**, 125405 (2004).
[51]I. F. Torrente, K. J. Franke, and J. I. Pascual, J. Phys. Condens. Matter **20**, 184001 (2008).